Wake Measurement Downstream of a Hybrid Wing Body Model with Blown Flaps

John C. Lin,* Gregory S. Jones,* and Brian G. Allan*
NASA Langley Research Center, Hampton, Virginia, 23681, USA john.c.lin@nasa.gov

Bryan W. Westra† and Scott W. Collins‡
Northrop Grumman Corporation, El Segundo, California, 90245, USA

Cale H. Zeune§
Air Force Research Laboratory, Wright-Patterson AFB, Ohio, 45433, USA

Abstract

Flow-field measurements were obtained in the wake of a full-span Hybrid Wing Body model featuring steady blowing through internally blown flaps. The test was performed at the NASA Langley 14 × 22 Foot Subsonic Tunnel at low speeds. Off-body measurements were obtained with a 7-hole probe rake survey system. Three model configurations were investigated. At 0° angle of attack the surveys were completed with 0° and 60° flap deflections. At 10° angle of attack the wake surveys were completed with a slat and a 60° flap deflection. The 7-hole probe results further quantified two known swirling regions (downstream of the outboard flap edge and the inboard/outboard flap juncture) for the 60° flap cases with blowing at both angles of attack. Flow-field results and the general trends are very similar for the two blowing cases at nozzle pressure ratios of 1.37 and 1.56. High downwash velocities correlated with the enhanced lift for the 60° flap cases with blowing. Jet-induced effects are the largest at the most inboard station for all (three) velocity components due in part to the larger inboard slot height. The experimental data are being used for the validation of computational tools for high-lift wings with integrated powered-lift technologies.

1. INTRODUCTION

NASA's Subsonic Fixed Wing Project is pursuing technologies and the validation of tools to enable cruise-efficient (CE), short take-off and landing (STOL) aircraft. The enabling tools and technologies are dual use in that they are applicable for both military and civilian purposes. As the result of a research and development collaboration between NASA Langley Research Center (LaRC), the Air Force Research Laboratory (AFRL), and the Northrop Grumman Corporation (Northrop Grumman), an all-wing aircraft with a blown-flap high-lift system, or the Hybrid Wing Body (HWB) concept, has emerged as a candidate to provide databases for the development of computational fluid dynamics (CFD) tools for the CE STOL efforts.

The inherent benefits of all-wing aircraft designs are well known in terms of cruise efficiency compared to conventional aircraft [1,2]. The HWB aircraft concept studied here leverages planform area while managing the risk in achieving the lift required for STOL operations. That is to say, if a low to moderate wing loading is chosen for conventional take-off and landing distances, then the amount of additional lift required for STOL objectives is minimized. The centerbody of the cuirent HWB concept produces one-third of the vehicle's total lift while the wings with internally blown flaps produce the remaining two-thirds [3].

A lot of research was performed on blown flaps in the past, both recently [3,4] and decades ago [5–9]. This pneumatic flow-control concept generally consisted of blowing a thin sheet of high-speed jet tangent to the flap's upper surface through a small slot near the flap's leading edge. This concept was successfully demonstrated for aerodynamic lift augmentation. As the thin jet is applied,

*Aerospace Engineer, Flow Physics and Control Branch, MS 170

†Manager, Propulsion System Design and Integration, MS 9V14/W6

‡Director, Future Tactical Systems, MS XE 40/W6

§Aerospace Engineer, AFRL/RBAA

the flow separation is moved aft along the flap surface, so the resulting lift improvement is due to "separation control". If the jet entraining and deflecting the airflow beyond the flap's trailing edge, then the resulting lift augmentation is due to "super circulation control", as reported by Jones et al. [4] where flow-field measurements were performed on a 2D airfoil with a blown dual-radius flap (circulation control) using Particle Image Velocimetry (PIV). However, there is no flow-field data available for the complex wake downstream of a 3D wing-body configuration using the blown flap system.

The currently reported joint NASA/AFRL/Northrop Grumman research efforts were conducted at the NASA Langley 14 × 22 Foot Subsonic Tunnel to examine a HWB model's high-lift performance. Part of these joint efforts involved a flow physics investigation using a 7-hole probe wake rake system to measure the off-body flow fields downstream of the model. The investigation was conducted to assess the complex flow interactions in the near wake of the blown flaps as well as to provide a flow-field database to the CFD community to evaluate computations. These data are being used in the development and validation of CFD tools to advance powered-lift/circulation-control technologies by contributing to the *"Subsystem Cases"* of AIAA's four-step code validation process adopted by NASA [10]. The process includes experiments documenting *Unit Problems, Benchmark Cases, Subsystem Cases,* and *Complete System* [11]. Collins, et al. [3] reported the incremental lift and surface pressure data of the HWB model. This paper will focus only on the results of the wake measurements and flow phenomena associate with this type of powered-lift system.

2. FACILITY DESCRIPTION

The NASA Langley 14 × 22 Foot Subsonic Tunnel is an atmospheric, closed return tunnel with a test section of 4.42 m (14.5 ft) high, 6.63 m (21.75 ft) wide, and 15.24 m (50 ft) long, a maximum freestream velocity of 103 m/s (338 ft/s), and a dynamic pressure (q) of 6.89 kPa (144 psf). The Reynolds number (Re) ranges from 0 to 7.2×10^6 per meter (2.2×10^6 per foot). Test section airflow is driven by a 12.19 m (40 ft) diameter, 9-bladed fan powered by a 12,000-hp solid-state converter with synchronous motor. The tunnel has a set of flow control vanes to maintain control of the speed for low-speed testing. The closed test section configuration was used for the current test, and the configuration produced relatively uniform flow with a velocity fluctuation of 0.1 percent or less [12]. The current flow-field investigation was conducted at a freestream Mach number (M_∞) of 0.143, a q of 1.44 kPa (30 psf), and a Re of 3.1×10^6 per meter (9.6×10^5 per foot).

3. EXPERIMENTAL SETUP

3.1 Model Description

The test article was a full-span sting-mounted model (see Fig. 1) with facility supplied high-pressure air for its internally blown flaps. The model was developed by Northrop Grumman for AFRL to advance the state-of-the-art of integrated high-lift and control technologies. The HWB

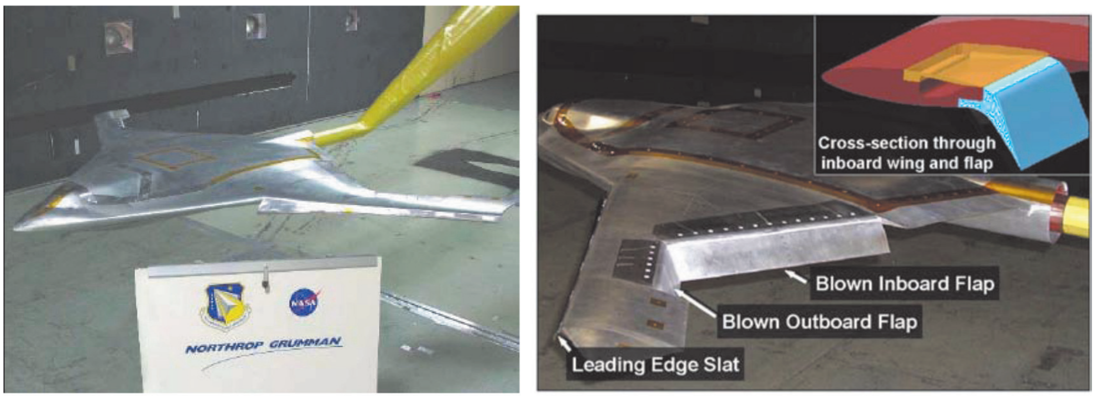

(a) Front side view (b) Rear side view showing 60º flaps

Figure 1. HWB Model in 14 × 22 Foot Subsonic Tunnel. (a) Front side view; and (b) Rear side view showing 60° flap.

model has a span of 2.44 m (8 ft), a length of 1.43 m (4.7 ft), and a mean aerodynamic chord of 0.84 m (2.75 ft). Trailing-edge flap deflections of 0° and 60° (downward) were used for the current investigation. Wake surveys were conducted with and without the baseline slat that has a 60° downward deflection. CFD and semi-empirical methods were used to determine the grit size and location. Specifically, this method considered the magnitude of the suction peak and subsequent adverse pressure gradient to determine transition on the full-scale configuration. Grit size was determined using a Northrop Grumman semi-empirical method based on the model scale, grit location, and test conditions. The analysis concluded that a strip of No. 60 grit (0.29 mm) located 25.4 mm (1 inch) normal from the leading edge on the inboard section of the model would adequately force transition. The outboard section of the wing was not gritted since the presence of the slat will force natural transition. The same grit size and location was applied on the lower surface.

The model was mounted on a flow-through bent sting. The Langley balance 1621 was used to measure forces and moments on the model. Because of the high-pressure air needs, the model balance was used with the "air sting" support system to provide a non-metric to metric high-pressure air balance crossover. Air sting's outer shell and its adapters (at both ends) are non-metric and they support the model. The air sting's internal air piping is metric and its coiled design enables the passage of high-pressure air to the model's internal balance without adversely affecting the force measurement. Figure 2 shows the metric components of the model support system, which included air sting coil, accumulator, model, balance block, and balance.

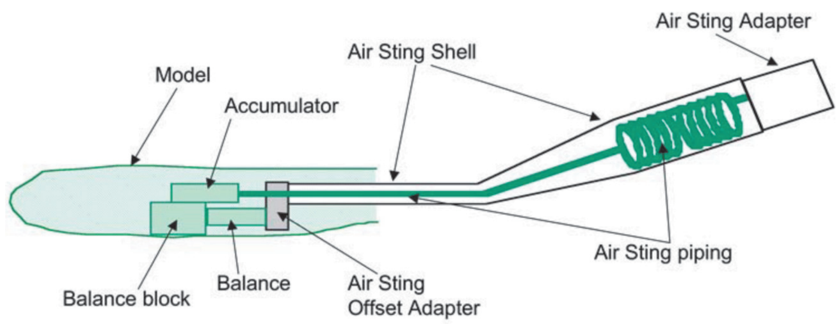

Figure 2. Air sting support components.

High-pressure air at approximately 1.59×10^3 kPa (230 psig) entered the model through a tube in the hollow support sting. The accumulator distributed air to high aspect ratio slots forward of the wing flap surfaces. There were four blowing slots, left-hand (LH) and right-hand (RH) inboard flaps as well as the LH and RH outboard flaps. Four distribution valves inside the model were used to control the nozzle pressure ratio (NPR) at each slot, where NPR is defined as the ratio of total pressure over freestream static pressure. The following NPR conditions were investigated in this study with the corresponding blowing coefficient ($C\mu$) [19] listed in parenthesis: 1.0 (0 or "blowing off'), 1.37 (0.034), and 1.56 (0.048). The purpose of the steady blowing was to ensure flow attachment on the flaps (i.e., separation control). Jones et al. [4] reported that a fully attached flow (or the end of separation control) on a blown flap was achieved with a $C\mu$ of 0.029. It is believed that the current blowing could be in the transition region between separation control and super circulation control.

The outboard flap had a constant-height slot (h_{OB}). The inboard blowing slot was linearly tapered in height (h), starting with $h = 4 \times h_{OB}$ at the inboard edge and transitioning to h_{OB} at the outboard edge. Porous choke plates were used to manage flow at each blowing slot. The choke plates were designed to create a large pressure drop from the facility air supply to the set total pressure at the slot nozzle, as well as to provide uniform, total pressure across the entire slot width for both the tapered inboard slot and the constant height outboard slot. The Mach number is sonic ($M = 1$) for exit NPRs above approximately 1.03. Therefore, because the slot flow rate varies linearly with pressure, the choke plates, once calibrated, can be used as accurate flow meters for each slot. The summation of all four calculated choke plate flows was also compared against the facility flow meter. Typical agreement was within +/–2% for the test.

3.2. 7-Hole Probe Flow Field Survey

Aerodynamicists have employed a variety of different types of multi-hole probes for flow diagnostics in complex flow fields. The 7-hole probe technique used in this study involves a standard, well-documented method of defining a set of non-dimensional coefficients based on the location of the maximum of the seven pressure readings from the probe [13–18].

The current probes were fabricated and calibrated by Aeroprobe Corporation. Each probe provides the three components of velocity for flow angles as high as 75° with respect to the probe's axis. These probes are rugged, and once calibrated require minimal maintenance to achieve an accuracy that is typically within 1% of the measured flow speed and 0.5° in flow angles. These accuracies are also dependent on the pressure transducer accuracy, typically less than 0.1% of full-scale.

The current 7-hole probe system is made up of a rake head holding eight 7-hole probes with a vertical spacing of 25.4 mm (one inch) between probe tips as well as a positioning system traversing 1001 mm (39.4 inches) in the horizontal spanwise (y) direction and 305 mm (12 inches) in the vertical (z) direction, as shown in Fig. 3. The 7-hole probe measurements were obtained in the wake at selected horizontal streamwise (x) locations downstream of the left wing. The U-, V-, and W-velocity components are measured in the tunnel coordinate system, corresponding to velocities in the x, y, and z direction, respectively. Test results are to be presented in the non-dimensional coordinate system X, Y, and Z, where they correspond to x, y, and z respectively normalized by a length scale roughly equal to half the model span (or 1.27 m).

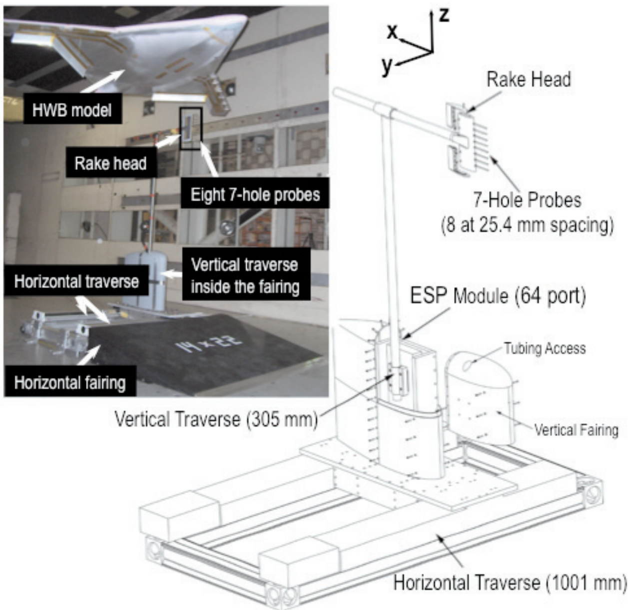

Figure 3. Wake rake survey system.

4. RESULTS AND DISCUSSION

The wakes from three configurations of the HWB model with blown flaps were investigated with the 7-hole probes. The three configurations were: A) 60° flap deflection, leading edge slat-on, and α (angle of attack) = 10°, B) 0° flap deflection at $\alpha = 0°$, and C) 60° flap deflection at $\alpha = 0°$. All configurations were at 0° yaw angle. Case A has the most resolution in the survey grid and included several survey stations in the X direction. Because of the time constraint towards the end of the test, the latter two cases, B and C, have fewer points in the grid than A. Flow features observed from the wake survey are discussed in the following sections.

4.1. Case A: 60° Flap and Slat-On at α = 10°

Once flow control is established, the flow features and aerodynamic performance were found to be very similar between the two blowing cases (NPR = 1.37 and 1.56). As a typical example, Figure 4 shows the results from Collins et al. [3] where the increases in lift coefficient produced by a single inboard flap blowing for 60° flap deflection at NPR = 1.4 were at least 85% as effective as those of NPR = 1.6 throughout the entire lift curve. It is believed that NPR = 1.4 is sufficient enough to achieve the flow separation control goals for Case A.

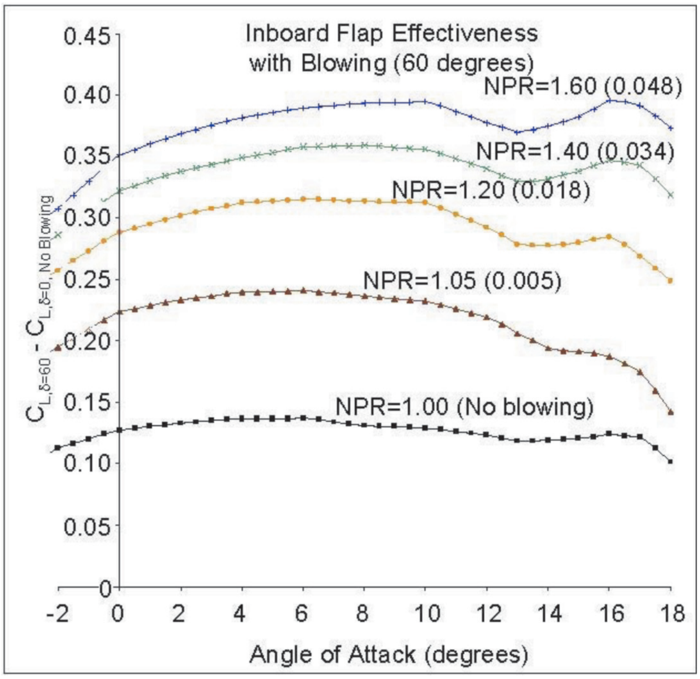

Figure 4. Effectiveness of blowing on increasing lift performance for a single inboard flap at 60° deflection (From Figure 7 of Collins et al. [3]).

Since the lower blowing case has an obvious advantage in pneumatic supply system requirements, only NPR = 1.37 results are presented in this section and are considered as representative of the blown flap case for this model. The flow-field data at X = 1.08 for the 60° flap and baseline slat-on model configuration at α = 10° are shown in Fig. 5, where X = 1.08 corresponds approximately to the trailing edge apex of the outboard wing (see the left sketch on top of Fig. 5). The data are presented in terms of streamwise mean velocity (U) contours and velocity vectors in the Y-Z (cross-flow) plane for NPR of 1.0 (non-blowing) and 1.37. The right sketch on top of the figure shows the location of the cross-flow measurement plane relative to the model. White boxes in the middle of the vortex or wake indicate high angularity in the local flows. Flows near the core of a wake vortex or near the off-body re-circulating regions could have flow angles greater than 75° with respect to the probe axis, which are outside the measuring capability of the 7-hole probes.

For NPR = 1.0 (Fig. 5 (a)), the large velocity deficit in the U-velocity contours between Y = –0.66 and –0.74 corresponds to the wake vortex associated with the outboard edge of the outboard flap. For the inboard flap, the velocity deficit is concentrated downstream of its inboard half and is considerably smaller towards the juncture between the inboard and outboard flaps (Y = –0.57). This may be due to the inboard wing trailing-edge forward-sweep increasing the distance from the flap to the survey plane. There also appears to be a weak juncture-induced swirling slightly towards the inboard side. The location of the swirling is perhaps influenced by the inboard moving spanwise flow dominating the upper portion of the wake. Notice that the inboard/outboard flap juncture was sealed (i.e.. no gap).

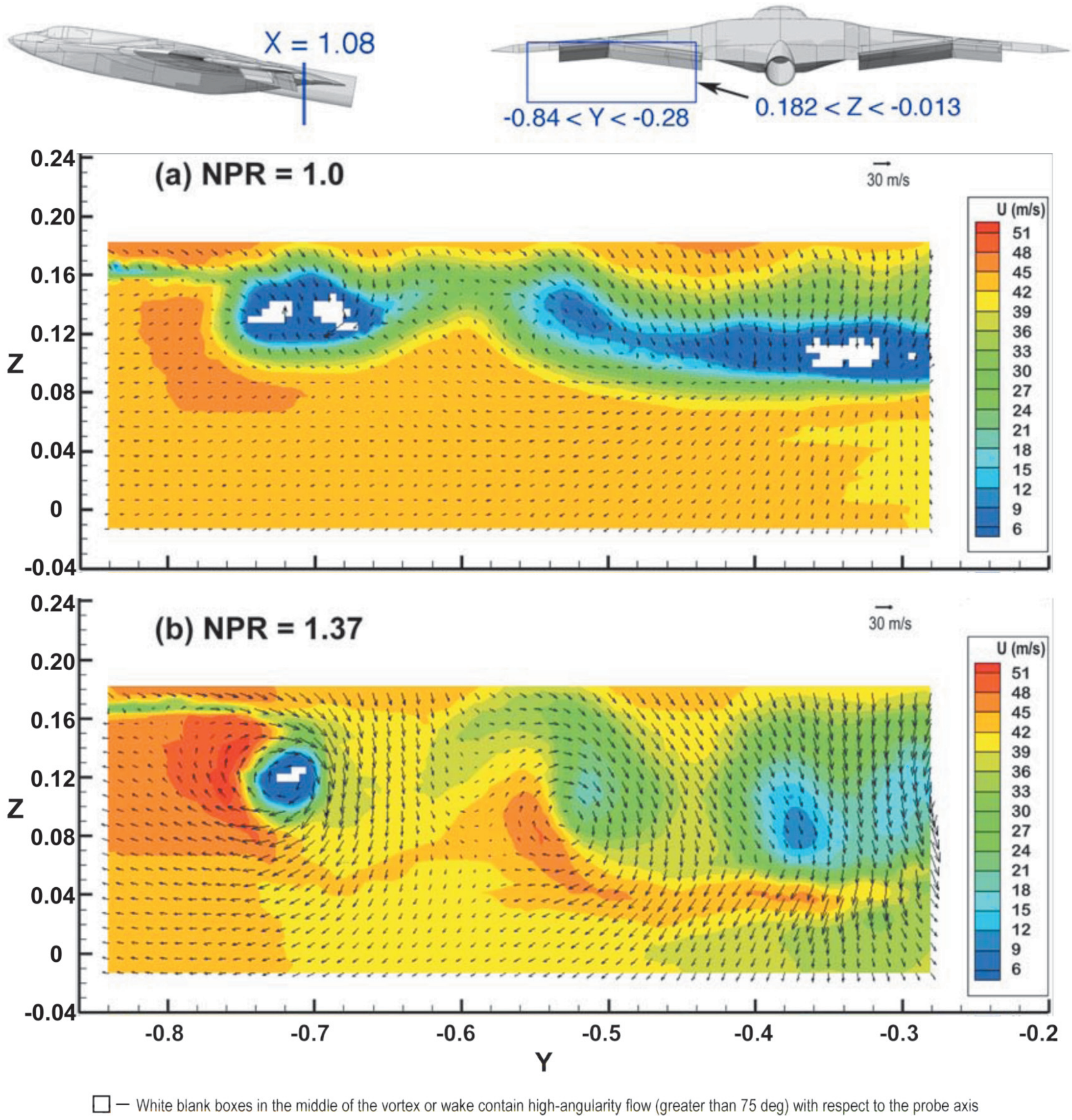

Figure 5. U-velocity contours and velocity vectors in Y-Z plane at X = 1.08 (M_∞ = 0.143, 60° flap and slat-on, α = 10°). (a) NPR = 1.0; and (b) NPR = 1.37.

For NPR = 1.37 (Fig. 5 (b)), the velocity vectors clearly show two swirling regions in the Y-Z plane. The increased lift (loading) and the effects of blowing jets significantly enhanced the strength of the (stronger) flap-edge-induced outboard vortex and the (weaker) juncture-induced swirling, centered at approximately Y= –0.72 and –0.53, respectively. The weaker swirling has significantly less velocity deficit in its core than the stronger (outboard) vortex. When viewing towards the upstream direction, the swirling motion is clockwise. The outer edge of a third vortex caused by the inboard edge of the inboard flap can be observed at the right side of the plots, but the main part of the vortex was just outside of the survey area. The expected inboard flap edge vortex has a counter-clockwise rotation when viewing upstream. The swirling vortices of the blowing case segmented the wake into several three-dimensional structures.

Flow-field results for the blowing case are presented in Fig. 6 in terms of Y-Z plane contours at X = 1.08 for the velocity magnitude (Vmag), the ratio of probe total pressure over freestream total pressure (Pt/Pto), and the streamwise vorticity. Vmag takes all three velocity components into account. Combination of Vmag and total pressure contours are good indicators of blowing strength locations within the measuring plane. The results indicate concentrated regions of high Vmag and Pt/Pto located at $Z \approx 0.04$ near the inboard flap (see Figs. 6 (a) and 6 (b)). These high Vmag and Pt/pto regions resulted from the significant effect of momentum addition from the inboard blowing jet. The U-velocity component of Fig. 5 is smaller compared to the Vmag of Fig. 6 (a) in regions above and below the inboard jet sheet. This indicates that a significant amount of downwash velocity exists, as expected for the high-lift system. The high degree of flow turning is also seen in the vector field plot. The streamwise vorticity plot (Fig. 6 (c)) confirms the two regions of concentrated negative vorticity associated with the two known swirling regions (downstream of the outboard flap edge and downstream of the inboard/outboard flap juncture). Two small pockets of concentrated positive vorticity, which might be associated with the inboard flap-edge-induced vortex, are also observed near the bottom right region of the plot.

For NPR = 1.0 and 1.37, the U-, V-, and W-velocity distributions along the Z-axis (vertical) are shown in Figs. 7 and 8, respectively. The Part (a) of each figure shows the U-velocity profile, while Parts (b) and (c) show the V- and W-velocity profiles, respectively. The plots along the three rows show the three spanwise stations of Y = –0.42, –0.57, and –0.65, while the plots along the four columns show the four X stations of 0.99, 1.08, 1.16, and 1.24. The sketches at the top of each figure show the location of these (X, Y) stations with respect to the model, where the blue lines also indicate the extent of the survey in the vertical direction. According to the defined coordinate system, positive V-velocity represents inward flow towards the fuselage and negative represents outward flow towards the wing tip; similarly, positive W-velocity represents upward flow and negative represents downward flow. For clarity, the freestream value (~48 m/s) for the U-velocity and the zeros for V- and W-velocity were marked in these plots as references.

The U-, V-, and W-velocity profiles are distinctive from one another at each measuring location. Figures 7 (a) and 8 (a) show that the U-velocity deficits in the wake were largest nearest to the model (X = 0.99) and grew smaller, as expected, as the wake moved farther away. For both blowing (NPR = 1.37) and non-blowing (NPR = 1.0) cases, the U-velocity deficits decreased more rapidly downstream of the outboard flap (Y = –0.65) when compared to those of the juncture (Y = –0.57) or inboard flap (Y = –0.42) stations. Perhaps this is due to the enhanced mixing produced by the swirling vortices observed in Figs. 5 and 6, where the blowing case showed significant spreading of the wakes in the Z-direction and distinctive "S-shaped" U-velocity profiles (see Figure 8 (a)). The bottom half of the S-shaped profile is due to the momentum addition of the blowing jets where their effect is strongest nearest to the model.

Figures 7 (b) and 8 (b) show that the V-velocities are generally positive (inward flow) in the top portion of the surveys, with negative velocities (outward flow) in the bottom portion. The magnitudes of the V-velocities in both directions are generally larger for the blowing case due to the stronger lift and vortices present in the flow field, which enhanced the inward flow on the top and outward flow on the bottom. The boundaries between the inward and outward flows are also generally lower for the blowing case.

The W-velocities are mostly negative (downwash flows), as shown in Figs. 7 (c) and 8 (c). Small regions of up-wash flows are noted near the middle portion of the survey ($Z \approx 0.08$ to 0.14) for the non-blowing case and downstream of the juncture (Y = –0.57) station for the blowing case. The high negative values are another indication of enhanced lift due to the blown flap. The downwash magnitudes are largest downstream of the inboard and outboard stations nearest to the model for the blowing case. In fact, as seen in Fig. 8 (c) at X = 0.99 and Y = –0.42, the magnitude of the downwash velocity exceeds the value of the freestream velocity.

4.2. Case B: 0° Flap without Slat at $\alpha = 0°$

After measuring the flow field of the 60° flap and baseline slat configuration, the slat was removed from the model and the trailing-edge flaps were set to 0° deflection. Taking the flow-field data without the slat simplified the model geometry and removed the need to simulate the complex flows in the slat region. This isolated the flap-blowing effects for code validation/development. The velocity vectors in the Y-Z plane at X = 1.26 are shown in Fig. 9 for NPR = 1.0, 1.37, and 1.56 cases at $\alpha = 0°$, where X = 1.26 approximately corresponds to the trailing edge of the model fuselage (see the left sketch on top of Fig. 10).

Again, the sketch at the top of Fig. 9 shows the spanwise locations and the extent of coverage in the vertical direction of survey stations with respect to the model. As expected, Fig. 9 (a) shows relatively small velocity components in the Y-Z plane for the non-blowing case (NPR = 1).

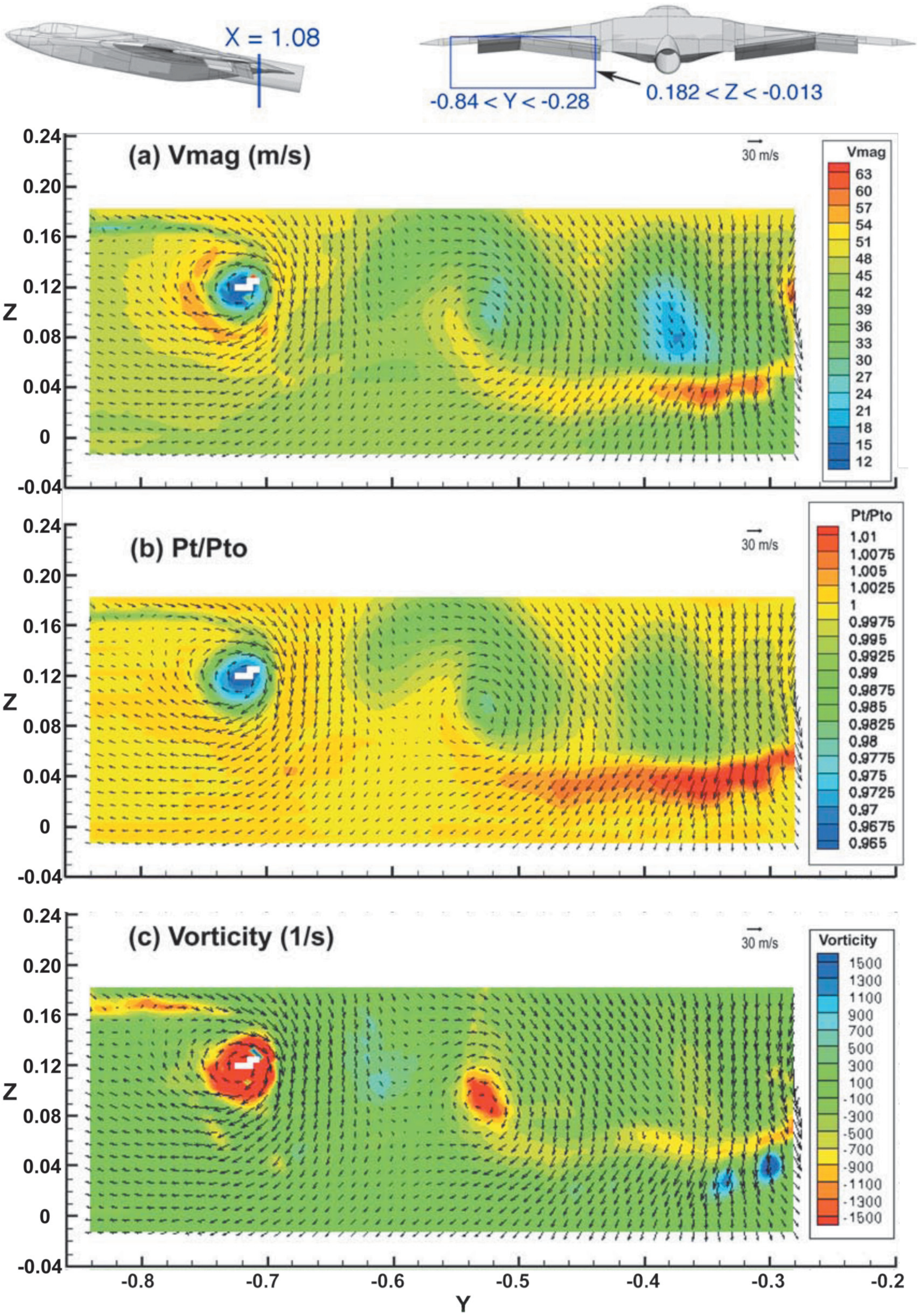

Figure 6. Vmag, Pt/Pto, and vorticity contours in Y-Z plane at X = 1.08 (M_∞ = 0.143, 60° flap and slat-on, α = 10°, NPR = 1.37). (a) Vmag; (b) Pt/Pto; and (c) Streamwise vorticity.

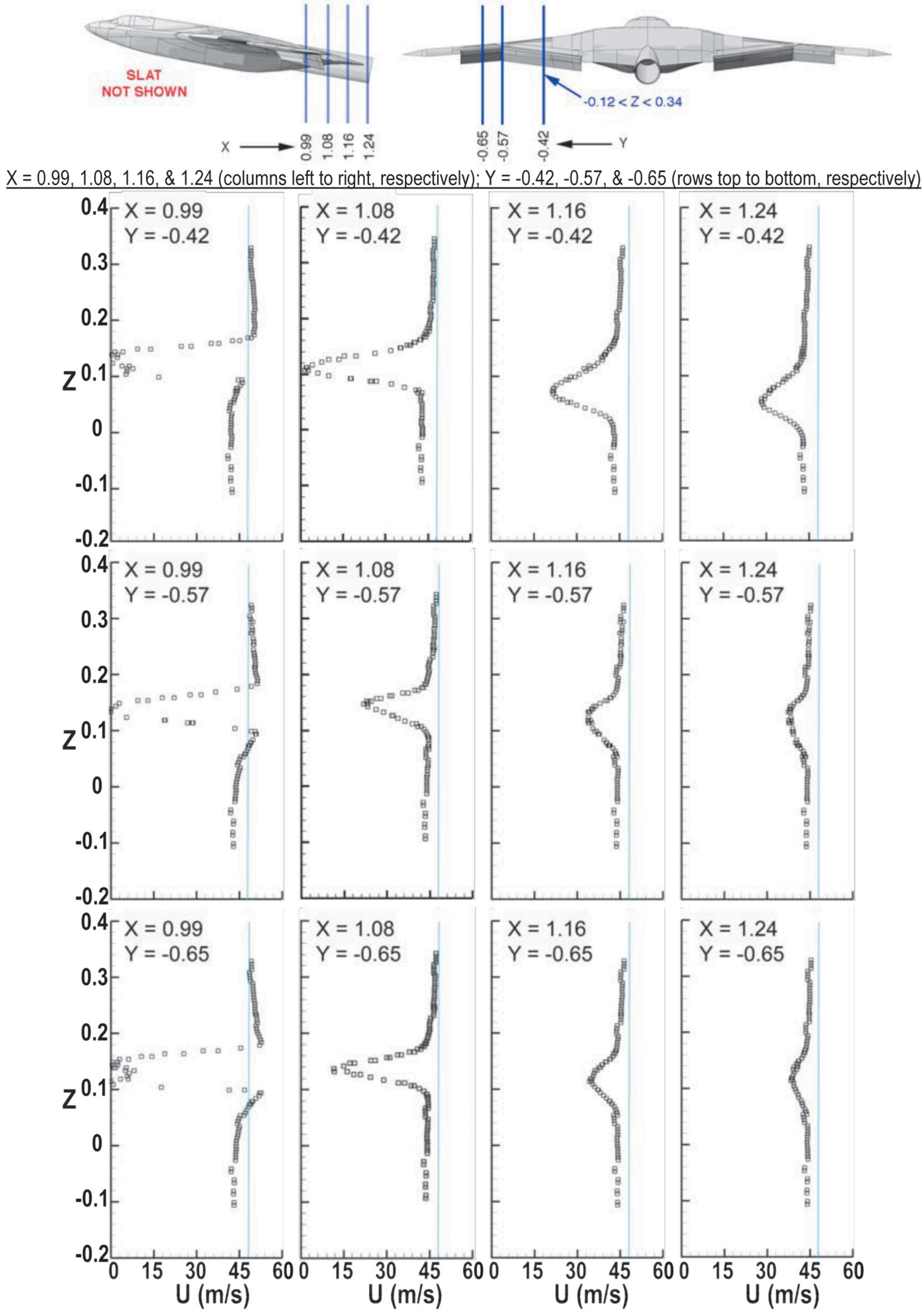

(a) U-velocity profiles

Figure 7. U-, V-, and W-velocity profiles for 60° flap and slat-on model at NPR = 1.0 (M_∞ = 0.143, α = 10°). (a) U-velocity profiles; (b) V-velocity profiles; and (c) W-velocity profiles.

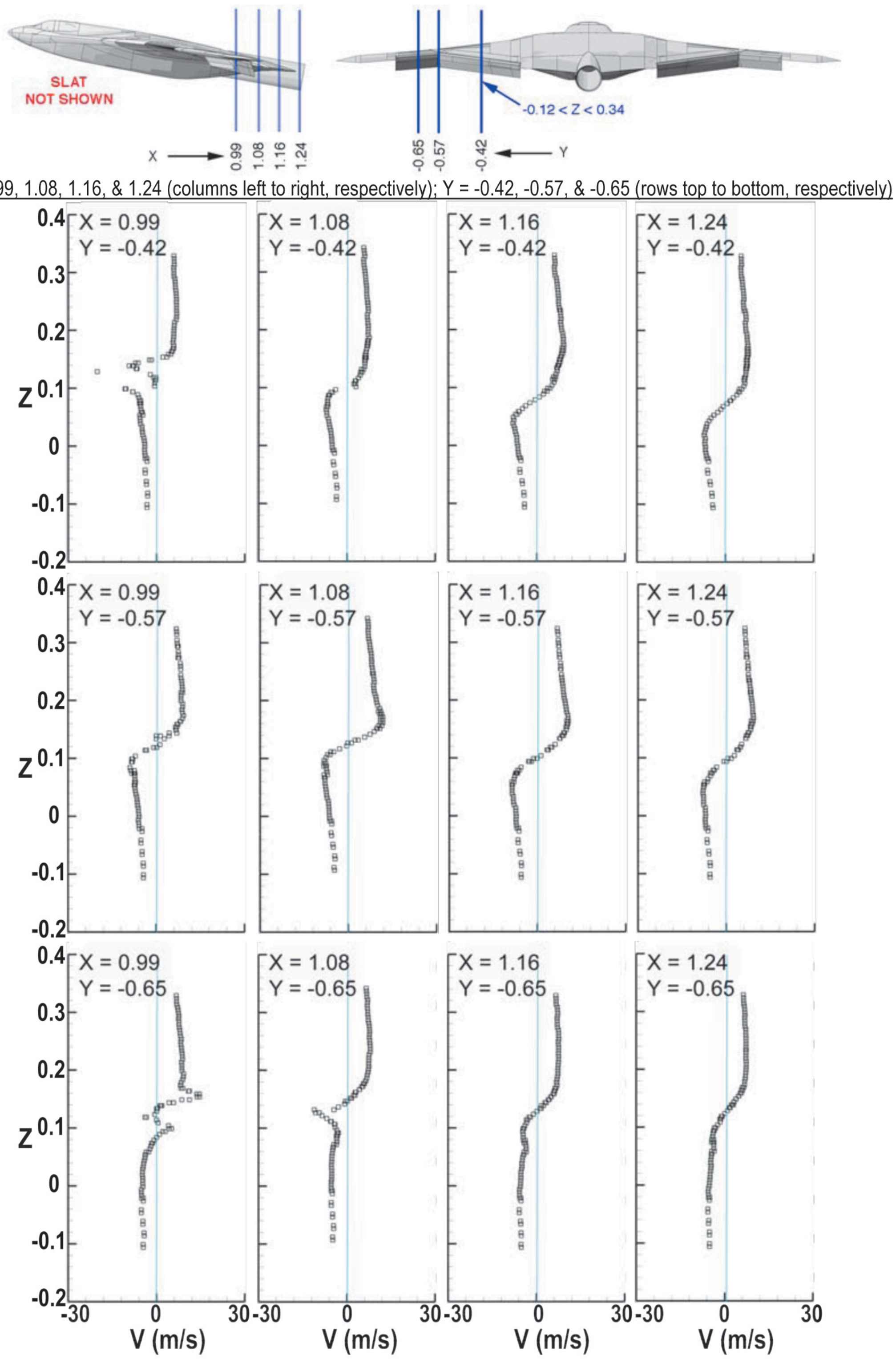

(b) V-velocity profiles (+ represents flow towards inboard, - represents flow towards outboard)

Figure 7. Continued (NPR = 1.0).

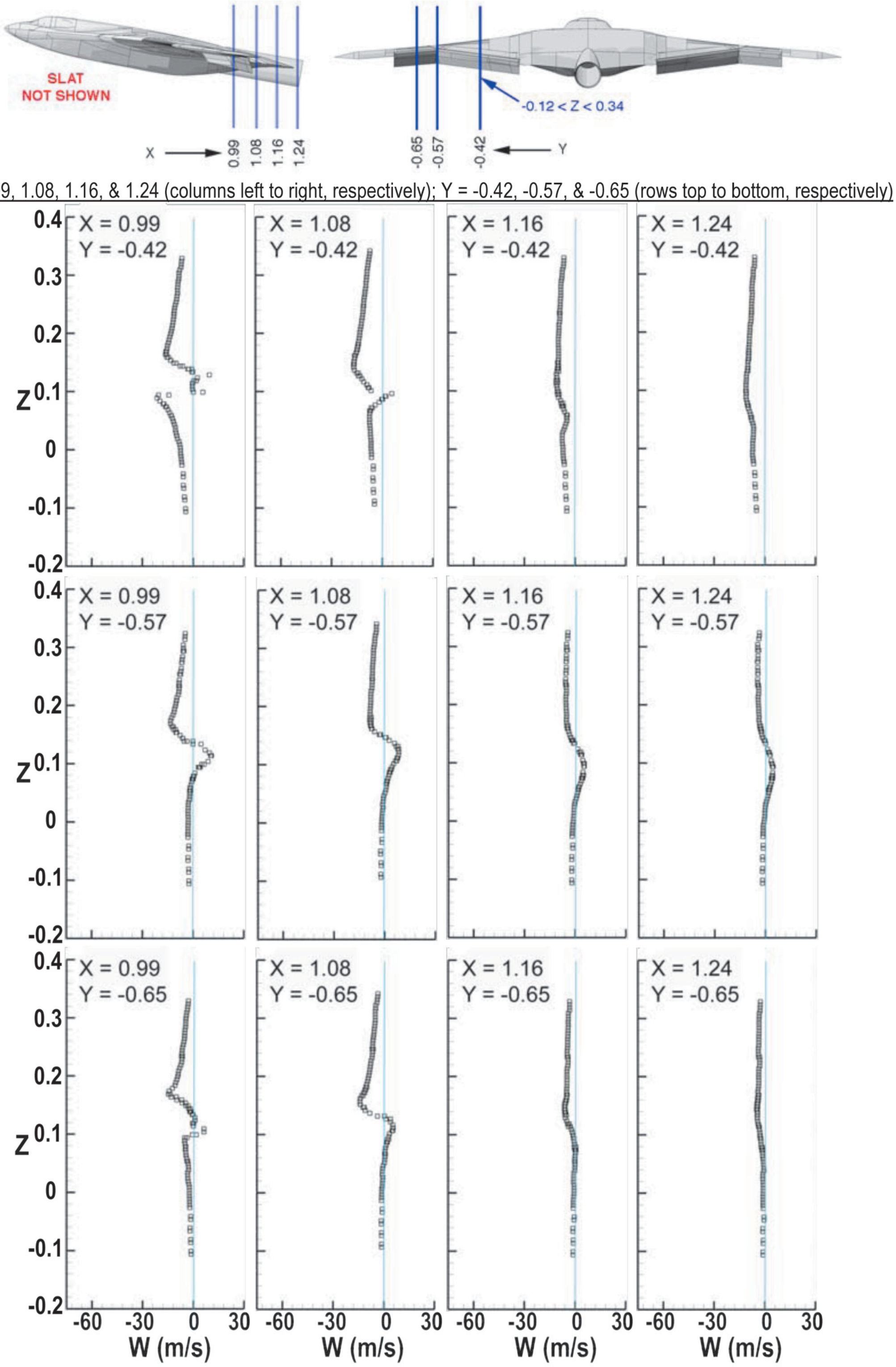

(c) W-velocity profiles (+ represents upward flow, - represents downward flow)

Figure 7. Concluded (NPR = 1.0).

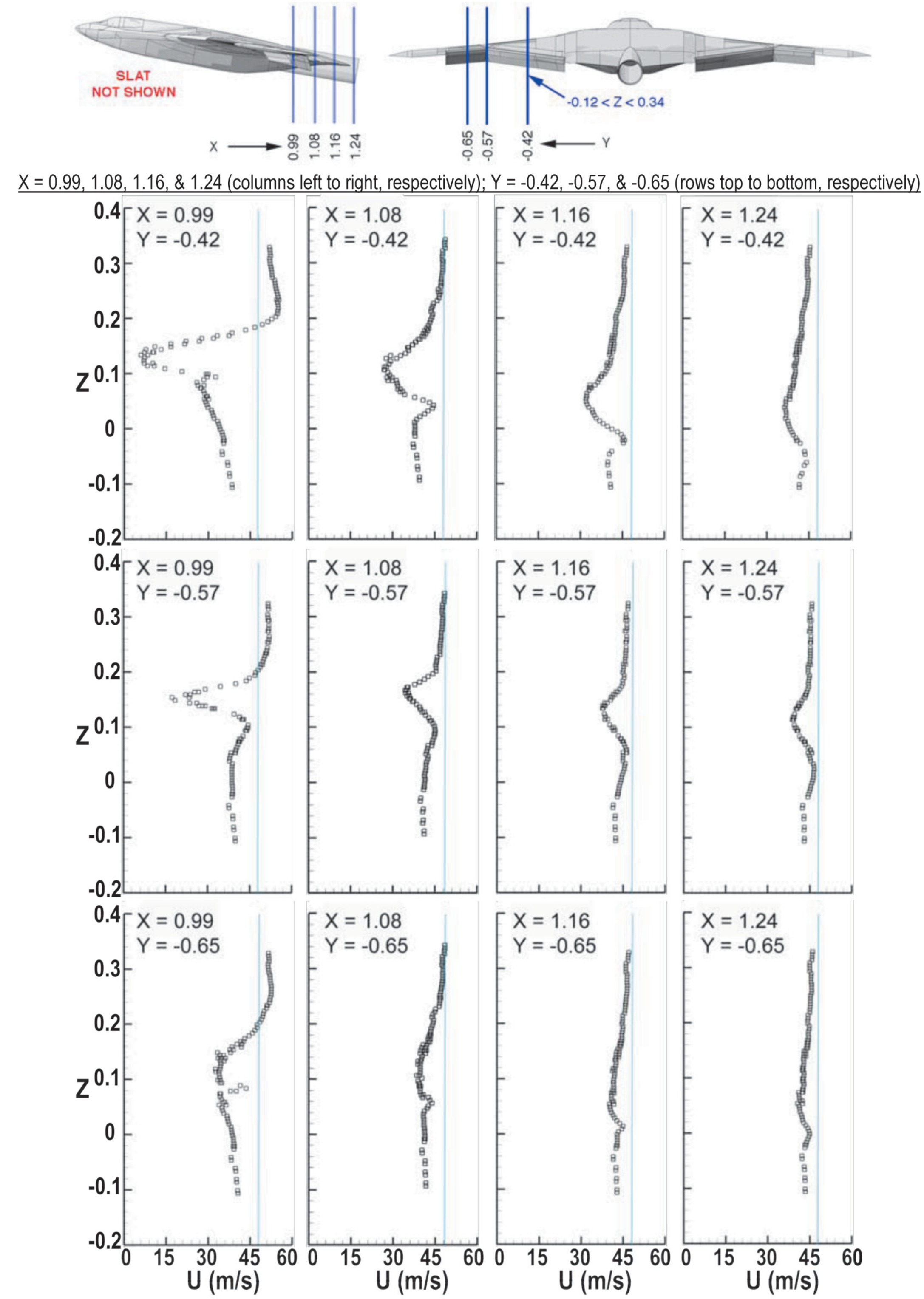

(a) U-velocity profiles

Figure 8. U-, V-, and W-velocity profiles for 60° flap and slat-on model at NPR = 1.37 ($M_\infty = 0.143$, $\alpha = 10°$). (a) U-velocity profiles; (b) V-velocity profiles; and (c) W-velocity profiles.

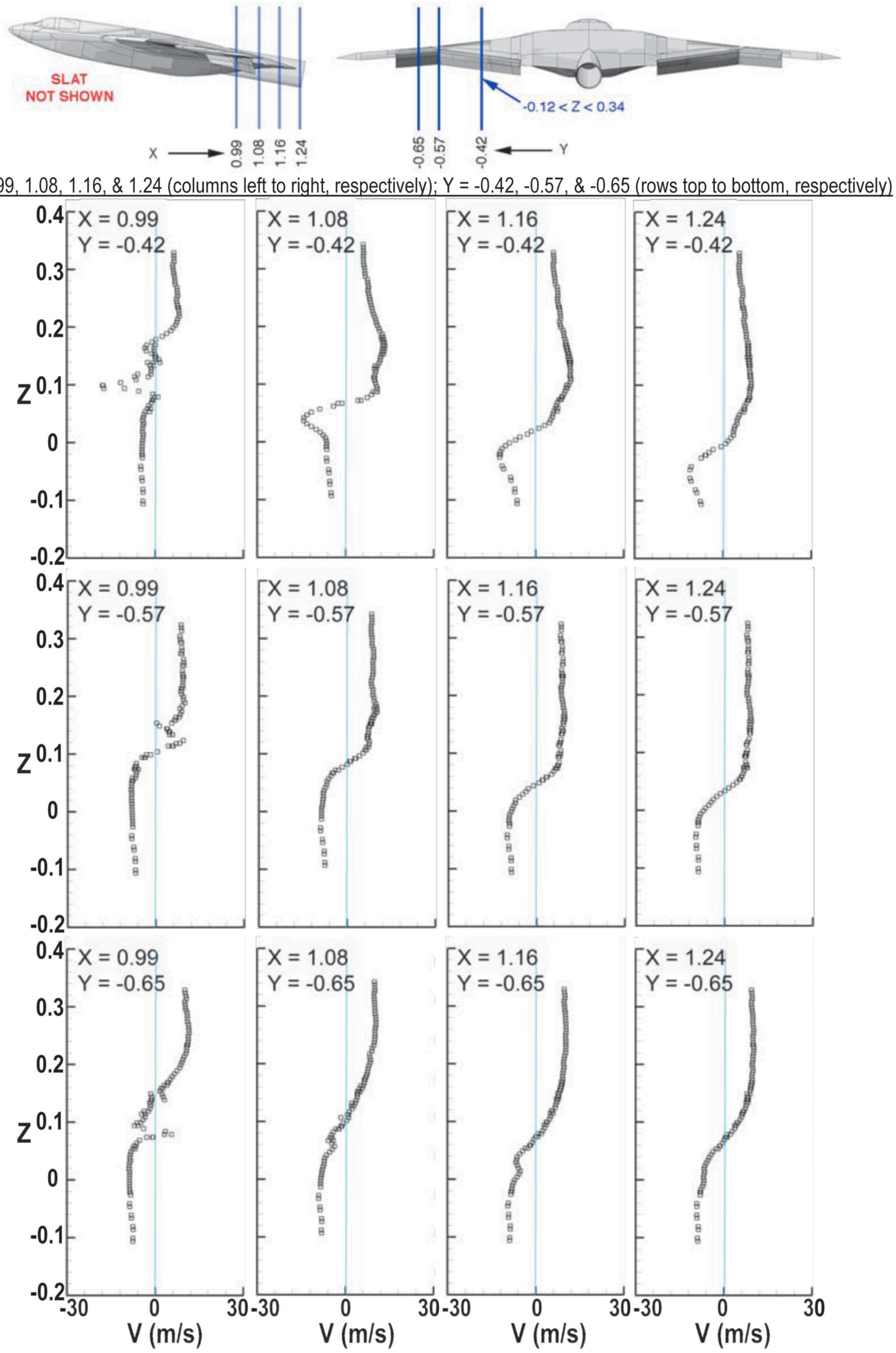

(b) V-velocity profiles (+ represents flow towards inboard, - represents flow towards outboard)

Figure 8. Continued (NPR = 1.37).

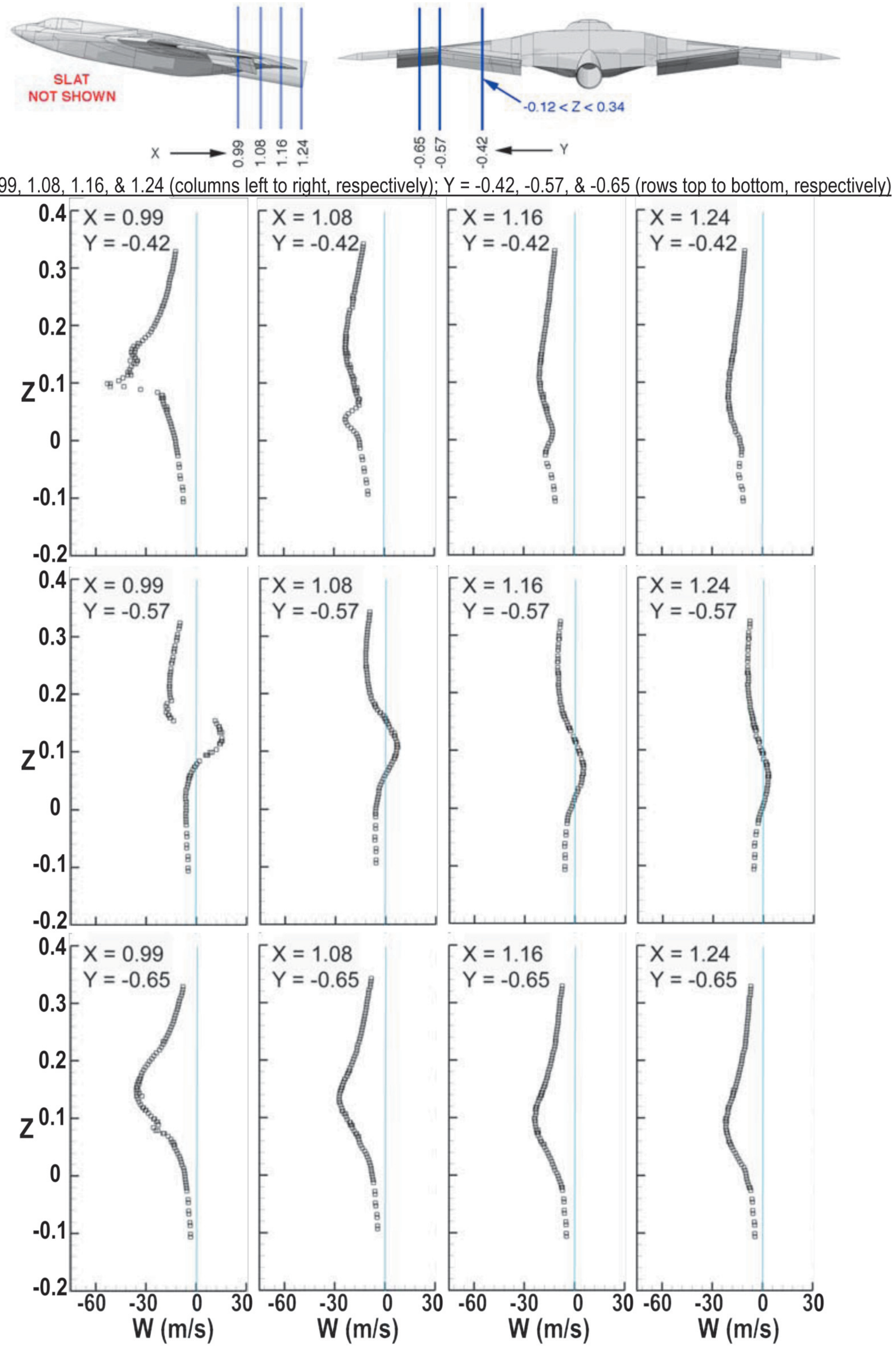

(c) W-velocity profiles (+ represents upward flow, - represents downward flow)

Figure 8. Concluded (NPR = 1.37).

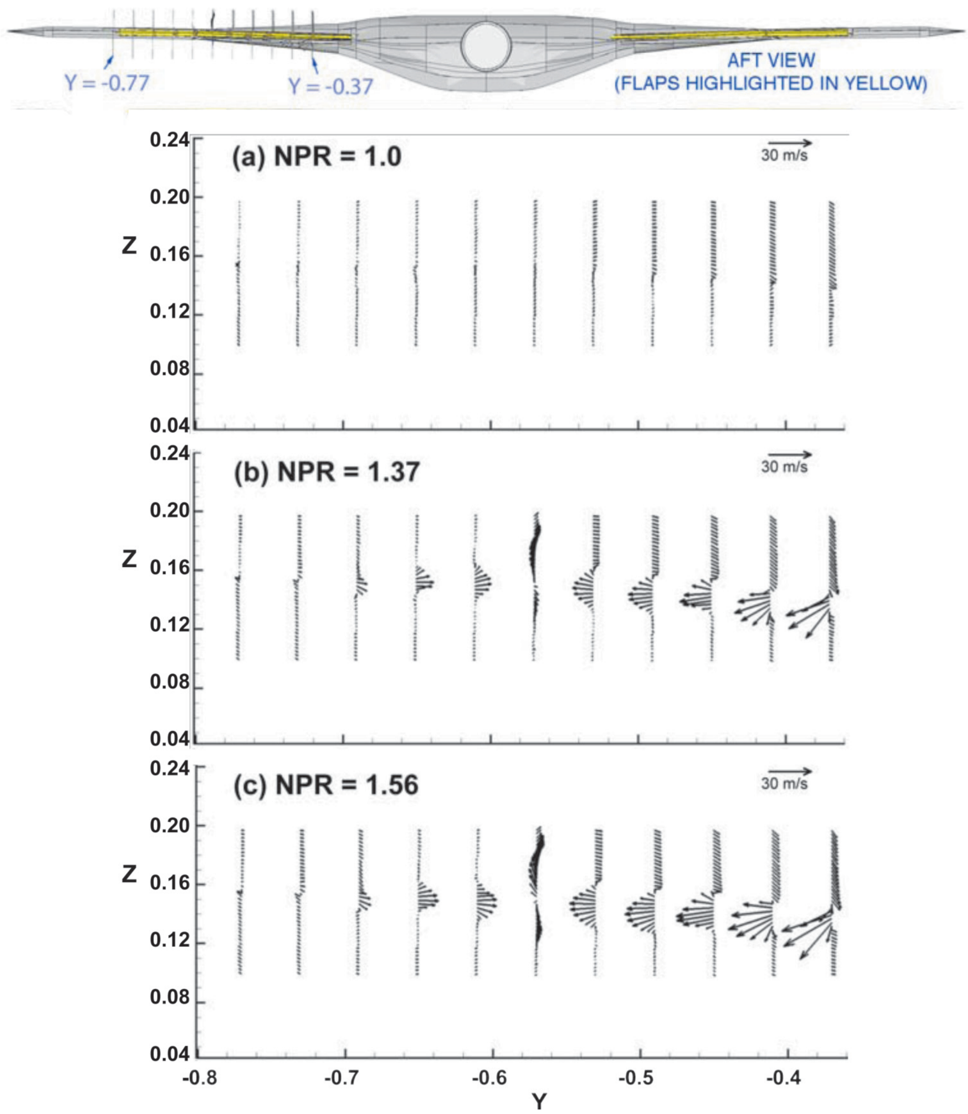

Figure 9. Velocity vectors in Y-Z plane for 0° flap without slat ($M_\infty = 0.143$, $\alpha = 0°$, X = 1.26). (a) NPR = 1.0; (b) NPR = 1.37; and (c) NPR = 1.56.

However, for both blowing cases, large velocity components are observed in the Y-direction, and to a lesser extent in Z-direction. The NPR = 1.56 case shows similar but slightly stronger velocity vectors than the NPR = 1.37 case at most stations as expected (see Figs. 9 (b) and 9 (c)). The jet effects are larger at the inboard flap stations in part because of the increased slot height and therefore increased blowing momentum, but also because the probes moved closer to the blowing slot as the survey moved inboard.

Figure 10 shows the U-, V-, and W-velocity profiles (top, middle, and bottom rows, respectively) for the NPR = 1.37 case at eight selected Y stations. For all stations, Fig. 10 (a) shows not only little or no U-velocity deficit but a significant increase in the local U-velocity (almost 1.6 times the freestream value) due to momentum addition from the blowing jets. The theoretical jet velocity magnitude (Vjet) at the slot exit is 225 m/s ($V_{jet}/U_\infty \approx 4.6$).

The V-velocity profiles in Fig. 10 (b) show inward flow for the two Y stations (Y = –0.61 and –0.69) downstream of the outboard flap and outward flow for the five Y stations downstream of the inboard flap (Y = –0.37, –0.41, –0.45, –0.49, and –0.53). This was expected because the internal blowing plenum is designed to supply flow perpendicular to the wing trailing edge. Because of the swept trailing edges, the V-velocity should be approximately $V = V_{jet} \times \sin(\Lambda_{TE})$, where Λ_{TE} is the corresponding trailing-edge sweep angle that is negative for the inboard flap and positive for the outboard flap. The

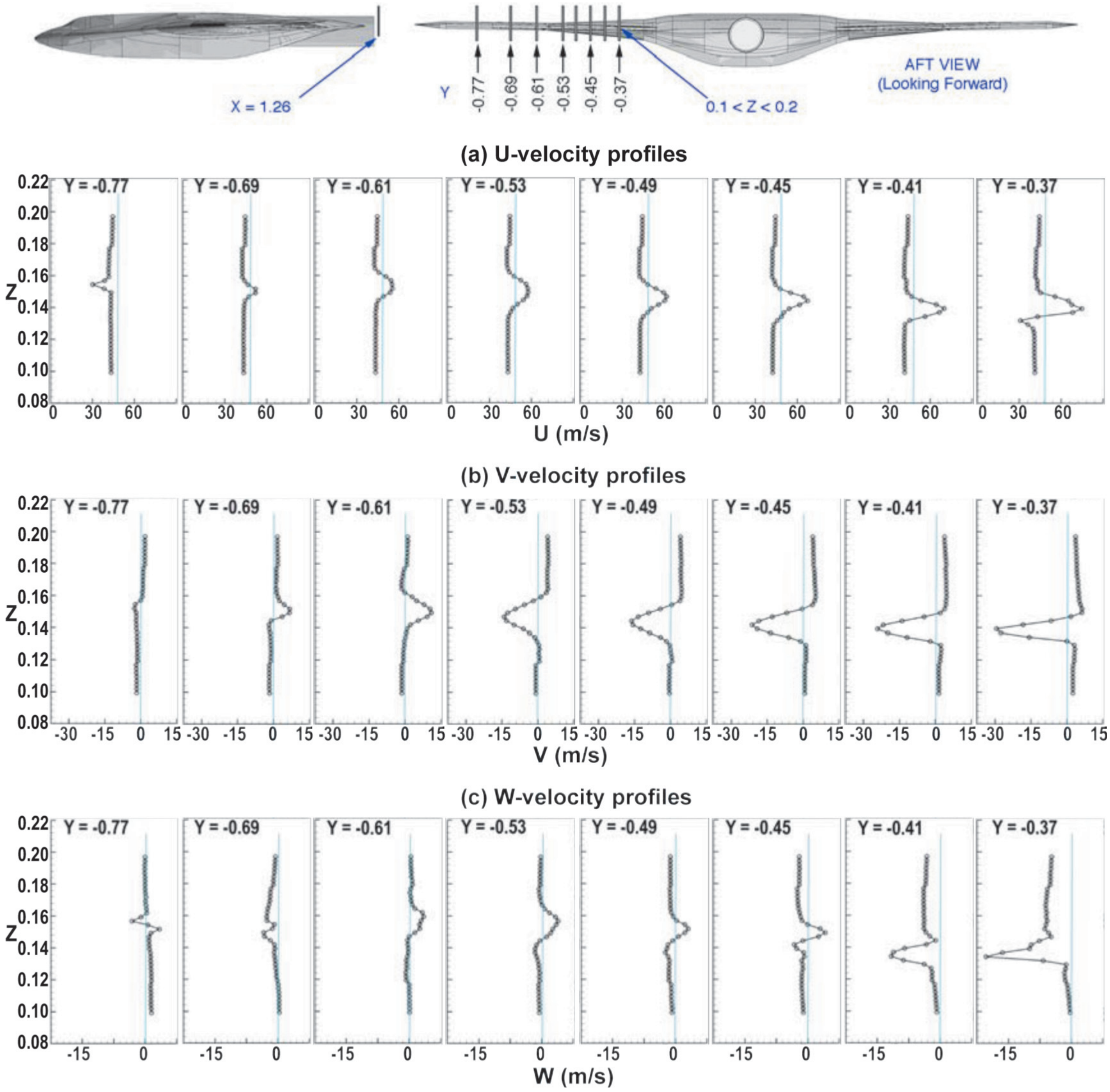

Figure 10. U-, V-, & W-velocity profiles for 0° flap without slat at various Y stations (M_∞ = 0.143, α = 0°, X = 1.26, NPR = 1.37). (a) U-velocity profiles; (b) V-velocity profiles; and (c) W-velocity profiles.

W-velocity profiles in Fig. 10 (c) show a small up-wash region near the middle portion of the survey (Z ≈ 0.14 to 0.16) for most cases, except for the two most inboard Y stations (Y = –0.37 and –0.41) where the jet-induced downwash flows are most dominant.

As previously mentioned, the jet effects are the largest at the most inboard station for all U-, V-, and W-velocity profiles because of the increasing slot height and decreasing distance to the survey-plane as the trailing edge sweeps aft. There was no blowing upstream of the most outboard station (Y = –0.77), so the minor U-velocity deficit observed there is associated with a small wake from the outboard wing.

4.3. Case C: 60° Flap without Slat at α = 0°

The final case examined was the 60° flap deflection case without the slat. The velocity vectors in the Y-Z plane at X = 1.26 for the two blowing cases (NPR = 1.37 and l.56) at α = 0° are shown in Fig. 11. No 7-hole probe survey was conduced for the non-blowing case because of expected flow separation on the flap. A courser survey grid was used for the NPR = 1.37 case because of time constraints.

Figures 11 (a) and 11 (b) show the same general trend between the two blowing cases, where there appears at least two swirling regions similar to those of Case A in terms of the vortex magnitude, location, and direction of rotation.

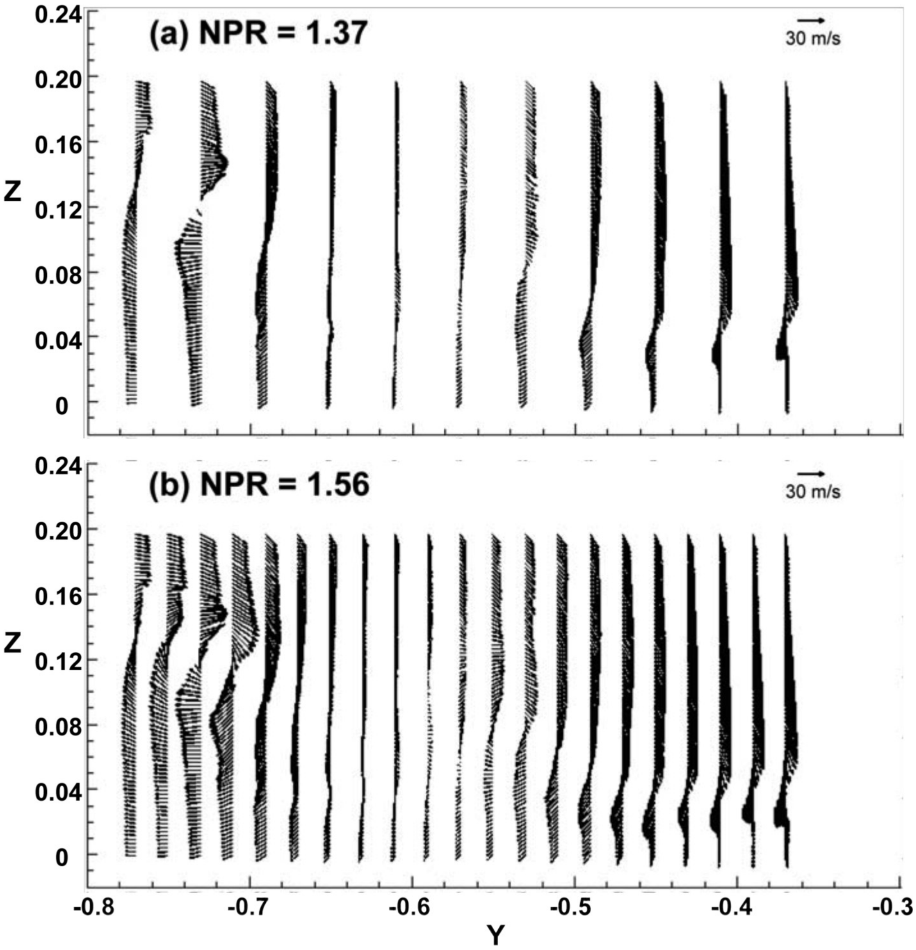

Figure 11. Velocity vectors in Y-Z plane for 60° flap without slat (M_∞ = 0.143, α = 0°, X = 1.26). (a) NPR = 1.37; and (b) NPR = 1.56.

Figures 12 (a), 12 (b), and 12 (c) show the U-, V-, and W-velocity profiles, respectively, for the NPR = 1.37 case at eight selected Y stations (see sketches at the top of the figure). No significant or obvious jet effect was observed for the U-, V-, and W-velocity profiles at the four most outboard Y stations. This is consistent with the data at X = 1.24, as shown in Fig. 8. Most likely the jet has mixed with the local flow at this point and eliminated the jet-induced shear layer.

For the four most inboard Y stations (Y = –0.37, –0.41, –0.45, and –0.49), Fig. 12 shows a continuing increase in the jet-induced U-, V-, and W-velocities, as the survey moved inboard. The U-velocity increased to almost 25 percent over the freestream and the W-velocity downwash approached the freestream value at the most inboard station (Y = –0.37). Again, the minor U-velocity deficit observed at Y = –0.77 is associated with a small wake from the outboard wing station that was outside of the blowing coverage.

5. CONCLUSIONS

Wake surveys using 7-hole probes were successfully performed on a full-span Hybrid Wing Body model featuring steady blowing through internally blown flaps at the NASA Langley 14 × 22 Foot Subsonic Tunnel. Three model configurations (60° flap deflection and slat-on with α = 10°, 0° flap deflection with α = 0°, and 60° flap deflection with α = 0°) and three NPR settings (1.0, 1.37, and 1.56) were investigated. The wake survey results significantly enhance the understanding of flow physics associated with this type of powered-lift system for HWB aircraft. Followings are some key results from this investigation:

(1) For the 60° flap cases with blowing, the power-lift system produced significant 3D flow field downstream, dominated by at least two streamwise vortices. The strength of the vortex

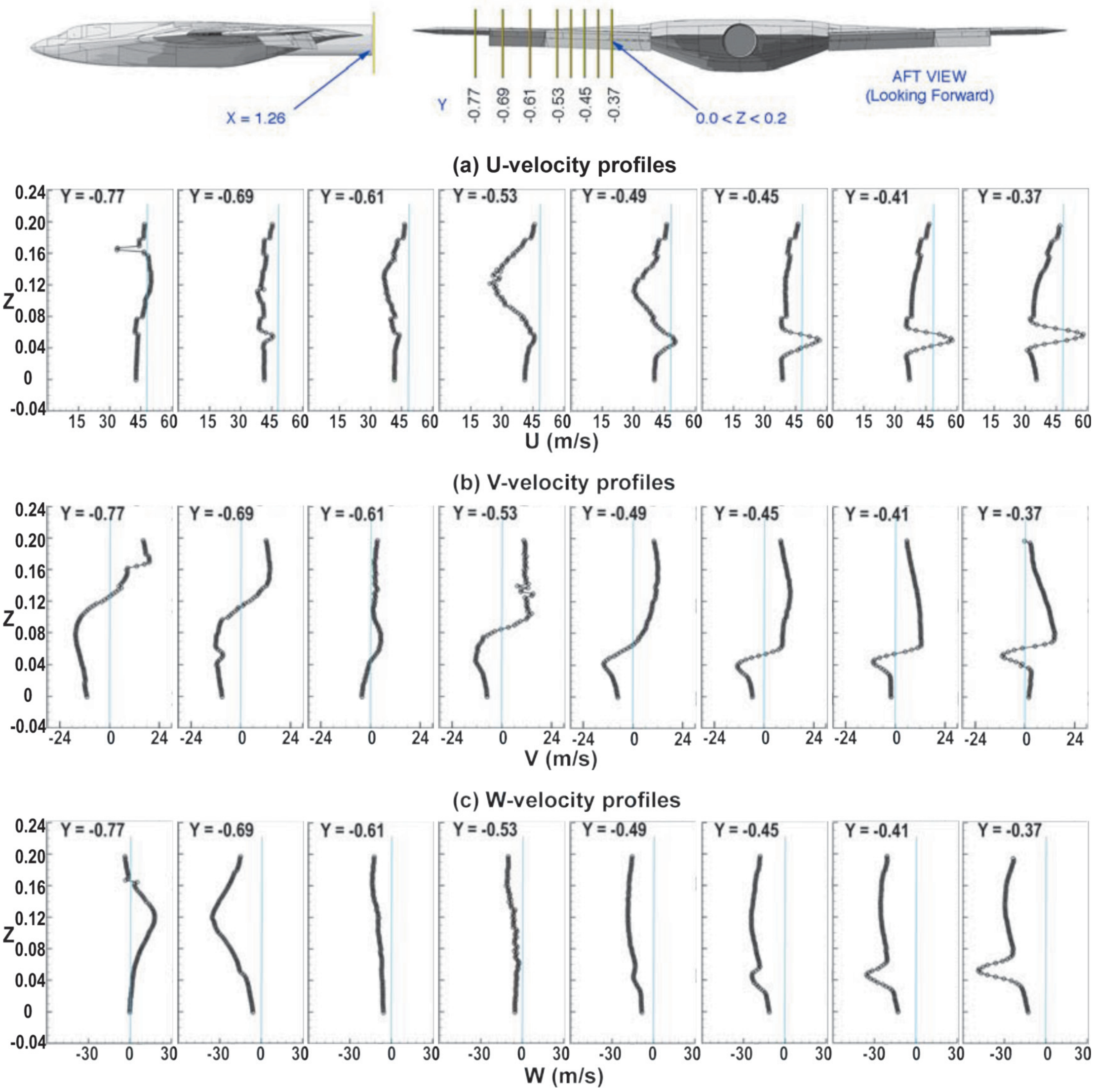

Figure 12. U-, V-, & W-velocity profiles for 60° flap without slat at various Y stations ($M_\infty = 0.143$, $\alpha = 0°$, X = 1.26, NPR = 1.37). (a) U-velocity profiles; (b) V-velocity profiles; and (c) W-velocity profiles.

downstream of the outboard flap edge was significantly stronger than the one downstream of the inboard/outboard flap juncture, where the juncture was sealed (i.e., no gap).

(2) Flow-field results and the general trends were very similar for the two blowing cases of NPR = 1.37 and 1.56. Although NPR = 1.56 was generally 10-15% more effective in lift enhancement than NPR = 1.37, however the lower blowing case (NPR = 1.37) has an obvious advantage in pneumatic supply system requirements and therefore more preferable.

(3) Velocity profile data indicated high downwash velocities corresponding to the enhanced lift for the 60° flap cases with blowing. Flap blowing also significantly enhanced the wake mixing downsteam.

(4) Jet-induced effects were the largest at the most inboard station for all three velocity profiles because of the increasing slot height (and thereby mass flow) and decreasing in distance to the survey-plane as the trailing edge sweeps aft.

Although the 7-hole probe technique has demonstrated its capability to identify complex and interesting flow features in the current study. It also has several drawbacks, such as: (a) measurements limiting to local flow angles less than 75° with respect to the probe axis, (b) long data acquisition time, (c) no turbulence measuring capability in the wake, and (d) its intrusiveness in the flow field. Using a widefield PIV system may help to overcome some of these issues. The model can also be improved by having less flow obstruction in the internal supporting structures that were used to maintaining the slot height. These are lessons learned and can be used to help to improve the future testing of similar models. The experimental data are being used to develop and validate CFD tools for high-lift wings with advanced powered-lift technologies.

ACKNOWLEDGMENTS

The authors extend their special thanks to the staff and crews of the NASA Langley Research Center 14- by 22-Foot Subsonic Tunnel and the AFRL/Northrop Grumman/NASA research team members for their contributions during this project.

REFERENCES

1. Northrop, J.K., "The Development of All-Wing Aircraft," presented at the 35th Wilbur Wright Memorial Lecture, May 1947.
2. Lieback, R.H., "Design of the Blended Wing Body Subsonic Transport," *Journal of Aircraft,* Vol. 41, No. 1, 2004, pp. 10–25.
3. Collins, S.W., Westra, B.W., Lin, J.C., Jones, G.S., and Zeune, C.H., "Wind Tunnel Testing of Powered Lift, All-Wing STOL Model," RAeS-566-5A3, *The Aeronautical Journal,* February 2009, pp. 129–137.
4. Jones, G.S., Yao, C-S, and Allan, B.G., "Experimental Investigation of a 2D Supercritical Circulation-Control Airfoil Using Particle Image Velocimetry," AIAA Paper 2006-3009, June 2006.
5. Riebe, J.M., "A Correlation of Two-Dimensional Data on Lift Coefficient Available with Blowing-, Suction-, Slotted-, and Plain-Flap High Lift Devices," NACA RM L55D29a, Oct. 1955.
6. Lachmann, G.V., *"Boundary Layer and Flow Control. Its Principles and Application,"* Volumes 1 and 2, Pergamon Press, New York, 1961.
7. Lawford, J.A., and Foster, D.N., "Low-Speed Wind Tunnel Tests on a Wing Section with Plain Leading- and Trailing-Edge Flaps Having Boundary-Layer Control by blowing," British Aeronautical Research Council R&M 3639, 1970.
8. Englar, R.J., and Huson, G.G., "Development of Advanced Circulation Control Wing High-Lift Airfoils," AIAA Paper 83-1847, July 1983.
9. Englar, R.J., Smith, M.J., Kelley, S.M., and Rover, R.C., "Development of Circulation Control Technology for Application to Advanced Subsonic Transport Aircraft," AIAA Paper 93-0644, January 1993. Also published in *Journal of Aircraft,* Vol. 31, No. 5, p. 1160–1177, Sept.-Oct. 1994.
10. Jones, G.S., Lin, J.C., Allan, B.G., Milholen, W.E., Rumsey, C.L., and Swanson, R.C, "Overview of NASA's CFD Validation Experiments for Circulation Control Application," RAeS– 566–8A1, presented at the 2008 International Powered Lift Conference, London, UK, July 2008.
11. Guide for the Verification and Validation of Computational Fluid Dynamics Simulations, AIAA G-077-1998 (2002).
12. Neuhart, D.H., and McGinley, C.B., "Free-Stream Turbulence Intensity in the Langley 14- by 22-Foot Subsonic Tunnel," NASA TP-2004-213247, 2004.
13. Johansen, E.S., Rediniotis, O.K., and Jones, G.S., "The Compressible Calibration of Miniature Multi-Hole Probes," *Journal of Fluids Engineering,* Vol. 123, No. 3, 2001, pp. 128–138.
14. Rediniotis, O.K., Hoang, N.T., and Telionis, D.P., "The Seven-Hole Probe: Its Calibration and Use," *Forum on Instructional Fluid Dynamics Experiments,* Vol. 152, 1993, pp. 21–26.
15. Zeiger, M.D., and Schaeffler, N.W., "Correcting Multi-Hole Probe Alignment Bias Errors Post-Calibration," AIAA Paper 2001 -0900, January 2001.
16. Epstein, R.J., Carbonaro, M.C., and Caudron, F., "Experimental Investigation of the Flowfield About an Upswept Afterbody," *Journal of Aircraft,* Vol. 31, No. 6, 1994, pp. 1281–1290.
17. Everett, K.N., Gerner, A.A., and Durston, D.A., "Seven-Hole Cone Probes for High Angle Flow Measurement: Theory and Calibration," *AIAA Journal,* Vol. 21, No. 7, 1983, pp. 992–998.
18. Zilliac, G.G., "Calibration of Seven-Hole Probe for Use in Fluid Flows with Large Angularity," NASA TM 102200, 1989.
19. Poisson-Quinton, Ph., and Lepage, L., "Survey of French Research on the Control of Boundary Layer and Circulation," in Lachmann, G.V., *"Boundary Layer and Flow Control. Its Principles and Application,"* Volume 1, pp. 21–73, Pergamon Press, New York, 1961.